Chemical Geology 467 (2017) 100–109

Contents lists available at ScienceDirect

Chemical Geology

journal homepage: www.elsevier.com/locate/chemgeo

Dissolution and surface roughening of Columbia River flood basalt at geologic carbon sequestration conditions

Rachel K. Wells[a,*], Wei Xiong[b], Daniel Giammar[b], Philip Skemer[a]

[a] Department of Earth & Planetary Sciences, Washington University in St. Louis, Campus Box 1190, One Brookings Drive, St. Louis, MO 63130, United States
[b] Department of Energy, Environmental and Chemical Engineering, Washington University in St. Louis, Campus Box 1180, One Brookings Drive, St. Louis, MO 63130, United States

ARTICLE INFO

Keywords:
Columbia River flood basalt
Carbon sequestration
Basalt dissolution
Surface roughening

ABSTRACT

Carbon storage in basalt reservoirs can mitigate CO_2 emissions to the atmosphere that contribute to climate change. For basalt reservoirs, CO_2 injection leads to Ca^{2+}, Fe^{2+}, and Mg^{2+}-rich solutions that may result in carbonate precipitation for long-term stable carbon sequestration. Examination of basalt surfaces as dissolution progresses can offer important information about which minerals are dissolving, the timing and sequence of dissolution, and the effects these processes have on surface roughness and morphology. We carried out two series of experiments using two polished Columbia River flood basalt samples in CO_2-rich water at 150 °C and 100 bar to observe the physical and geochemical changes during dissolution. One series reacted a sample over short time increments, while the other series examined a separate sample over longer time increments. Scanning electron microscopy, 2D profilometer analysis, and 3D laser confocal microscopy were combined with ICP-MS to characterize dissolution. Dissolution resulted in pitting, dissolution along fractures and grain boundaries, and an increase in species concentrations in the bulk solution over incremented reaction times. Based on these observations, early dissolution of olivine grains contribute Mg^{2+} and Fe^{2+} to aqueous solution in initial stages (< 1 week at a pH < 4), while slower continuous dissolution of Ca-rich pyroxene contributes Mg^{2+}, Fe^{2+}, and Ca^{2+} to the bulk solution over a longer period of time. The complete dissolution of olivine grains resulted in pits up to 200 μm deep. Dissolution of plagioclase and matrix was slower and resulted in the formation of micro-sized textures (< 10 μm). Following 1–2 months of reaction, the surface roughness parameters (mean and root mean squared) increased by factors of 42 and 28, respectively, while surface area of the flood basalt increased 20% relative to the starting polished surface. The results of this study indicate 1) pyroxene is the sustaining contributor of divalent metal cations during dissolution of basalt and 2) the limited connectivity limits of olivine and pyroxene grains the exposure of new reactive surface areas.

1. Introduction

Basalt dissolution is an important process in CO_2 sequestration in unconventional reservoirs such as large basalt flows (Gudbrandsson et al., 2014; IPCC, 2005; Matter et al., 2016; McGrail et al., 2017). Precipitation of carbonates within the reservoir depends on the availability of divalent metal cations that may dissolve from the basalt into the CO_2-rich solution or wet-CO_2 environment. Common minerals found in basalt, such as olivine, pyroxene, and plagioclase, can contribute several different divalent metal cations (e.g., Mg^{2+}, Fe^{2+}, and Ca^{2+}) into the CO_2-rich environment, which can lead to the formation of carbonate minerals (e.g., magnesite, siderite, and calcite).

The dissolution of basalt is more complex than that of single grains or rocks with homogeneous lithologies (e.g. limestone). Each mineral within the basalt dissolves at a different rate, and some minerals can release more than one divalent metal cation (Ca^{2+}, Mg^{2+}, Fe^{2+}). Sources of Mg^{2+} and Fe^{2+} are expected to be olivine (with end-member compositions of Mg_2SiO_4 – Fe_2SiO_4) or pyroxene (with end-member compositions of $Mg_2Si_2O_6$ – $Fe_2Si_2O_6$ – $Ca_2Si_2O_6$). Olivine is a favorable source of these divalent cations because dissolution is faster compared to pyroxene (Dixit and Carroll, 2007; Kelemen and Matter, 2008; Palandri and Kharaka, 2004; Rimstidt et al., 2012). While pyroxene dissolution is not as fast as olivine, all three relevant divalent metal cations can be sourced from this mineral. Ca^{2+} can also be sourced from plagioclase (with end-members compositions of $NaAlSi_3O_8$ – $CaAl_2Si_2O_8$) and the glassy matrix, which can be composed of a variety of cations; however, the dissolution rate of plagioclase and the glassy matrix is relatively slow (Chen and Brantley, 1997; Oelkers

* Corresponding author.
E-mail address: rwells@wustl.edu (R.K. Wells).

http://dx.doi.org/10.1016/j.chemgeo.2017.07.028
Received 12 May 2017; Received in revised form 24 July 2017; Accepted 27 July 2017
Available online 31 July 2017

and Schott, 1995; Palandri and Kharaka, 2004). The presence of the Ca^{2+}, Mg^{2+}, and Fe^{2+} noted in these basalt dissolution experiments (Gudbrandsson et al., 2011, 2008; Luhmann et al., 2017; Schaef and McGrail, 2009; Wolff-Boenisch et al., 2011) are generally attributed to the dissolution of olivine and/or pyroxene, but without microscopic examination, the interpretation of specific mineral dissolution in basalt is restricted to predicted dissolution rates and estimates based on mass balance calculations. Analyzing bulk solutions alone may not indicate which minerals are reacting as time progresses due to various dissolution rates and shared divalent metal cation sources, which limits our ability to predict dissolution rates in basalts of varied composition.

Evidence of dissolution is not limited to the presence of cations in the bulk solution, but also by the physical changes to the basalt surface. Broader-scale dissolution is primarily observed in experimental studies and models towards the inlet of a fracture or core (Elkhoury et al., 2013; Ellis et al., 2013; Luhmann et al., 2017; Singurindy and Berkowitz, 2005), while precipitation is often observed farther into the sample within diffusion limited zones (Andreani et al., 2009; Peuble et al., 2015; Singurindy and Berkowitz, 2005; Wells et al., 2017; Xiong and Giammar, 2014). As minerals dissolve, the porosity of the reservoir may increase depending on the flow rate and the characteristics of the pore structure (Luhmann et al., 2017). The preferential dissolution of specific minerals, due to fast dissolution rates or pre-existing structural heterogeneities (e.g., defects, twinning, chemical zoning), may result in heterogeneous pore development (Elkhoury et al., 2013; Ellis et al., 2013; Luhmann et al., 2017). For the most reactive minerals in basalt, preferential dissolution or weathering of olivine could result in localized pits (Olsson et al., 2012; Qafoku et al., 2012; Saldi et al., 2015). However, it is unclear if entire grains would be dissolved completely, leaving behind increased pore space and larger reactive surface areas. The surface area increase is also of particular interest to fluid transport models that use these observations to gage the validity of the carbonation potential in particular basalt formations.

The physical and chemical behavior of basalt in CO_2-rich environments strongly influences the potential for carbon storage as a permanent solution for mitigation of atmospheric CO_2 emissions. Matter et al. (2016) and McGrail et al. (2017) have shown that minerals in natural basalt reservoirs will dissolve and carbonates will precipitate within the formation. However, we do not fully understand how processes evolve at the water-surface interface. If we carefully examine the surface as the reaction progresses, we can clarify the specific source location of divalent metal cations over the course of the reaction, and the evolution of the surface topography. Our goal is to improve our understanding of basalt dissolution by better constraining the contributions of each mineral to cation contributions to aqueous solution and linking the dissolution of minerals to the evolution of surface roughness and surface area. In this study we reacted Columbia River flood basalt in water at 150 °C equilibrated with 100 bar CO_2, and we analyzed both the evolution of the fluid chemistry and surface of the samples. Analysis of the fluid chemistry was correlated with observations of the surface of the basalt over time to determine when certain minerals dissolved. Surface roughness was examined to characterize the effect of dissolution on fresh, unreacted surfaces.

2. Material and preparation

Flood basalt from the Columbia River Basalt Group, supplied by Wards Scientific and collected near Pullman, Washington, was used in this study (Table 1) Wells et al. (2016). The sample contains 9% (by volume) olivine (Fo_{60}) that is mostly unaltered, and 22% Ca-rich pyroxene. Olivine and pyroxene grains are subhedral, fractured, and have an average grain size of 75 and 88 μm, respectively. Olivine and pyroxene grains are rounded with an axial ratio of 1.6 and 1.5, respectively. Plagioclase grains and the K-rich matrix comprise 64% of the total volume; the remaining fraction is accessory phases, including illite. Plagioclase grains are euhedral and have an average grain size of 53 μm, although there are larger grains up to 400 μm long, and an axial ratio of 2.1. Plagioclase grains are zoned, with Na-rich rims and Ca-rich cores. The K-rich matrix is glass, and exhibits quench structures that are defined by Na-rich areas. Ilmenite grains are also common within the matrix (Supporting Information (SI) Fig. S1).

This study includes two series of experiments using two separate tile-shaped samples that were cut from the same flood basalt. Each side of a sample was polished using progressively finer SiC and diamond abrasives. The designated top surface was further polished with 0.04 μm colloidal silica to insure the smoothest starting surface to compare with subsequent reacted surfaces. One sample was used in a set of experiments (Series 1) that ran in cumulative increments of 1, 4, 7, 16, and 28 days. The dimensions of the Series 1 tile were $0.015 \times 0.013 \times 0.005$ m with an initial total surface area of 6.8×10^{-4} m^2. Series 1 used shorter reaction times to analyze the early stages of dissolution. The second sample was used in a set of experiments (Series 2) that ran for longer cumulative time increments of 7, 21, 35, and 56 days. Series 2 was used to examine effect of dissolution over longer periods of time. The Series 2 tile was slightly larger, with dimensions of $0.016 \times 0.014 \times 0.005$ m and an initial total surface area of 7.2×10^{-4} m^2. Two non-reactive epoxy markers were placed on opposite corners of each sample for a continuous reference throughout each series of experiments.

3. Experimental procedure

Each flood basalt sample was reacted in a CO_2-rich aqueous solution using the same procedure for each series of experiments (Fig. 1A). Each series began with a polished basalt sample that was reacted in a stainless steel 300 mL batch reactor with a PTFE liner. Each experiment used 190 mL of ultrapure water that was purged with nitrogen gas to minimize dissolved oxygen within the system. While flow or stirring of the solution can influence dissolution within a sample, each experiment was carried out under static conditions so that we could solely examine localized dissolution, which is dependent on the dissolution rate of each mineral present within the basalt. A Ti-wire basket was used to hold sample, which was placed into the basket with the epoxy markers facing upward. Two wire baskets were made, one for each sample. The same basket and sample pair were used throughout each series of experiments. Series 1 and Series 2 samples were reacted at 150 °C and 100 bar CO_2 for each increment within a series. For each experimental increment, the temperature was raised and then pressure was increased. The pressure usually stabilized within 1 h, indicating the water in the reactor was in equilibrium with the CO_2 in the headspace. The system was static (i.e., was not actively stirred) throughout each experiment. After each increment, the sample was removed, air dried (usually within 1 h), and then analyzed. All 190 mL of the reacted bulk solution was collected, and the reactor was then cleaned. Fresh (unreacted) water (190 mL) was then used for the start of the next increment.

The reacted bulk solution and top surface of each sample were analyzed after every increment. The concentrations of cations in the fluid were analyzed using inductively coupled plasma mass spectrometry (ICP-MS) (Perkin Elmer, Elan DRC II). The starting pH of the solution for every increment was calculated using a charge balance for water equilibrated with CO_2 at 150 °C and 100 bar, equilibrium constants calculated from the program SUPCRT92, and a CO_2 solubility calculated from Duan and Sun (2003). Following each experimental period, the measured cation concentrations from ICP-MS were then added to the charge balance calculation to determine the final pH of the reacted bulk solution. Surface roughness was measured using a 2D profilometer (KLA-Tencor Alpha – Step D-100). In addition, some samples were analyzed in more detail using a 3D laser confocal microscope (Keyence VK-X Series) (an unreacted polished tile, Series 1 sample reacted for 1 and 4 days total, and Series 2 sample reacted for 56 days total). The 2D roughness measurements were taken along the same general transect between two epoxy reference points; however,

Table 1
Starting material.

Mineral	Composition[a]	Total volume (%)	Grain size (μm)	Dissolution rate (mol/m^2/s)[b]	Dissolution study
Olivine	$Mg_{1.21}Fe_{0.78}SiO_4$	9	75	− 8.6	Forsterite: Rimstidt et al., 2012
Pyroxene	$Mg_{0.83}Fe_{0.48}Ca_{0.63}Al_{0.09}Si_{1.92}O_6$	22	88	− 9.0	Dioside: Palandri and Kharaka, 2004
Plagioclase	$Ca_{0.59}Na_{0.40}Fe_{0.03}Al_{1.57}Si_{2.40}O_8$	31	53	− 10.2	Labradorite: Palandri and Kharaka, 2004
Matrix	K-rich	33	–	− 15.3	Basaltic glass: Gislason and Oelkers, 2003
Ilmenite	$Ti_{0.68}$ $Fe_{0.64}Mg_{0.02}O_3$	3	–	− 17	Ilmenite: White et al., 1994

[a] Determined using WDS analysis from microprobe and EDS maps (Wells et al., 2016; Table 1S).
[b] Calculations based on 150 °C and a pH of 3.74.

due to the resolution of the instrument, the exact same transect was most likely not measured. The evolution of the surface area was estimated by comparing the actual 2D transect length to the starting 2D transect length of the unreacted sample. The mean roughness (Ra) was calculated using

$$Ra = \left(\frac{1}{L}\right)\int_0^L |z(x)|\, dx, \quad (1)$$

where L is the length of the transect and z is the height at a particular point along a 6 mm transect using the 2D profilometer data. The roughness root mean squared (RMS):

$$RMS = \left[\left(\frac{1}{L}\right)\int_0^L |z(x)|\, dx\right]^{1/2} \quad (2)$$

was also calculated (Petropoulos et al., 2010). The RMS parameter is more sensitive to minor peaks and troughs along a transect than is the Ra parameter, which is just a simple average of the topography and could represent many topographic profiles. The 3D surface area roughness (Sa – average of all surface values) was measured using the average height of a 200 × 200 μm area. For each parameter, a reported value at 0 indicates a perfectly smooth surface. Scanning electron microscopy (SEM) with secondary (SE) and backscatter (BSE) imaging was used to visually inspect dissolution textures and to monitor a single spot throughout each series. Energy dispersive spectroscopy (EDS) was used to get elemental composition that was used to identify minerals in each monitored area and any precipitates that formed.

4. Results

4.1. Ion sources during basalt dissolution

While each series was examined as a continuous set of experiments, the pH of each experiment within a series was not the same (SI Fig. S2). Every experiment began with fresh ultrapure water with a calculated pH of 3.4 at 150 °C and 100 bar CO_2. Equilibrium with CO_2 occurred within an hour. As the sample reacted and material dissolved into the bulk solution, the pH of the system rose. All of the bulk solution was collected at the end of an increment, and analyzed using ICP-MS to determine the cation concentration. The concentrations were then added to the charge balance for the final pH calculation of the solution. For both series of experiments, the overall system remained acidic. Overall, the final pH of each increment in Series 1 ranged from 3.6 to 4.2, while the final pH of each experiment in Series 2 ranged from 3.4 to 4.4 (Fig. 1B–C).

The cumulative cation release was calculated based on the measured concentrations of the 190 mL bulk solution following every experiment in each series (Fig. 2; SI Table S1). Due to the procedure used to document the dissolution of the flood basalt samples, the cumulative release values do not represent a reaction that reached equilibrium. The replenished solution and the low surface-to-volume ratio resulted in a solution that never became fully saturated and the experiment was far from equilibrium with respect to the dissolution of the primary minerals.

For every stage of the series, silicon had the greatest release to the bulk solution. The general trend of the silicon increased to a total

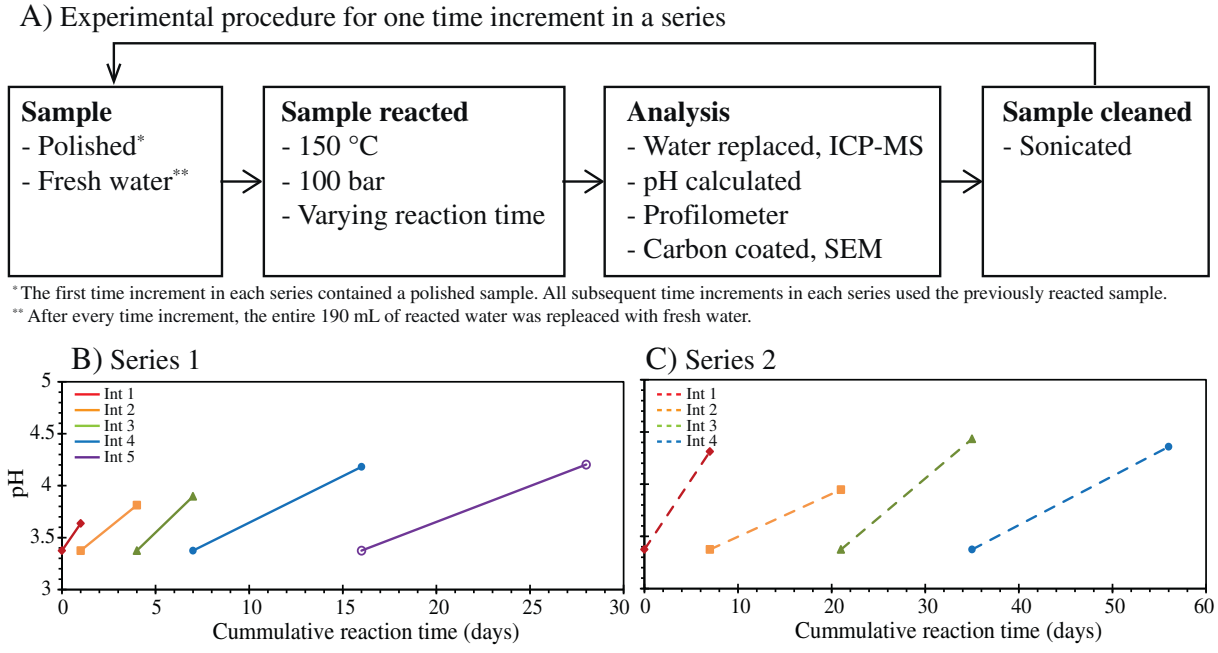

Fig. 1. Experimental procedure and pH. (A) Experimental procedure for each increment in a series. (B) The pH for Series 1 for each increment. (C) The pH for Series 2 for each increment.

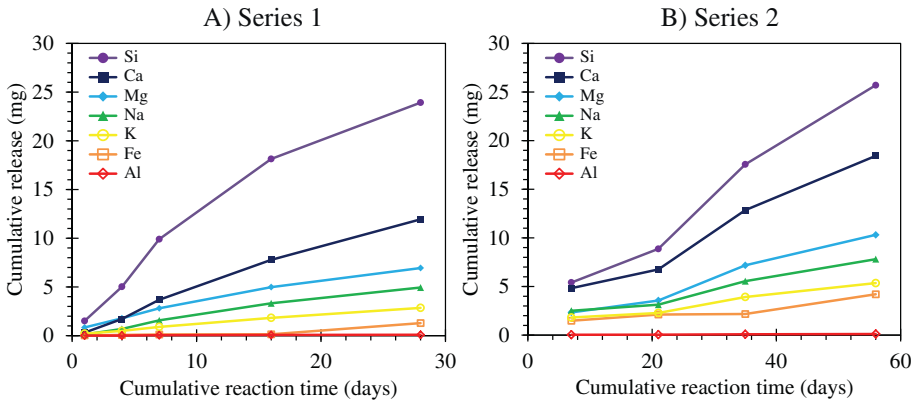

Fig. 2. Fluid chemistry. Cumulative release of species of each increment from the (A) Series 1 sample and (B) the Series 2 sample.

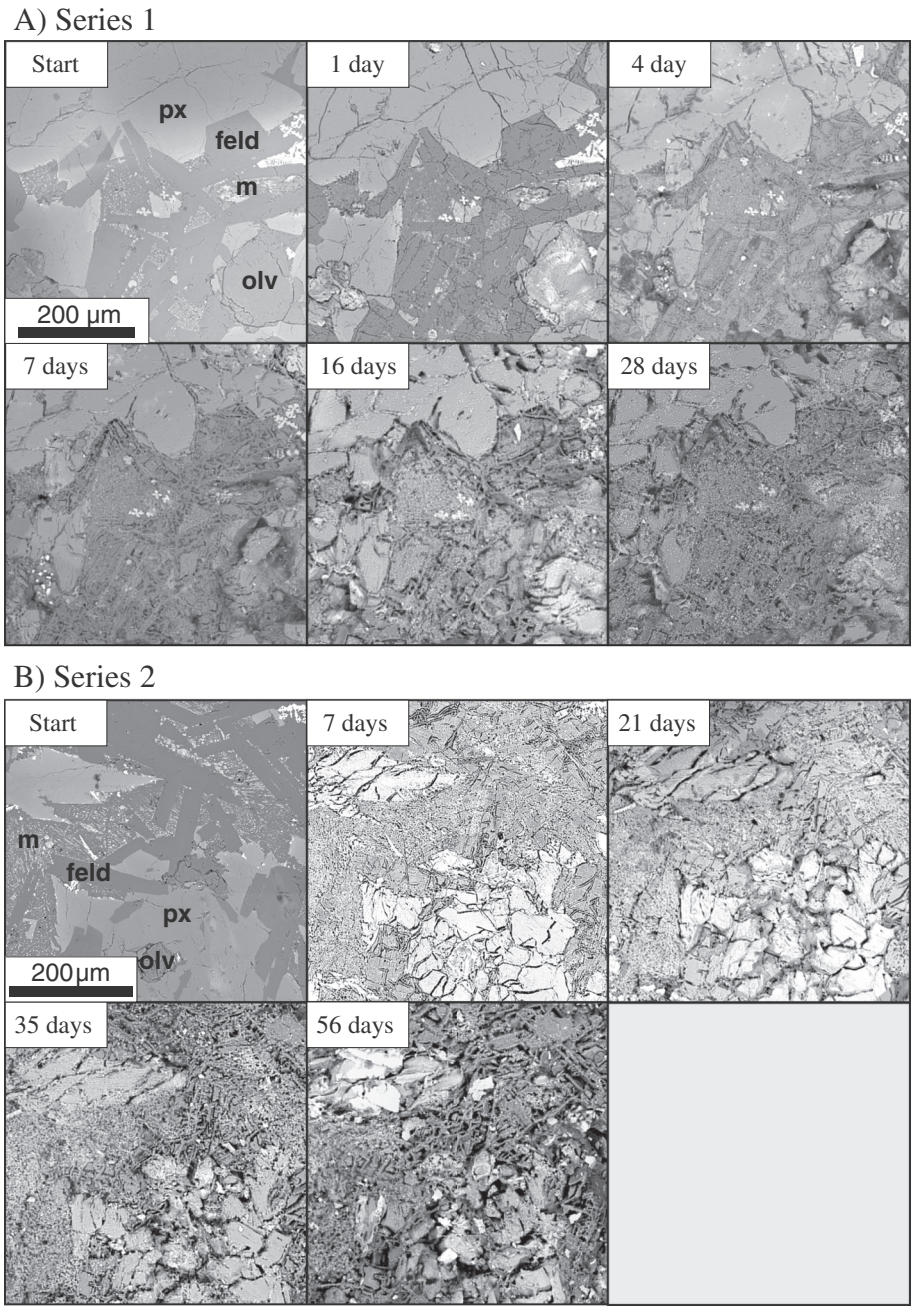

Fig. 3. Surface evolution. BSE images of (A) Series 1 and (B) Series 2 contain evidence of dissolution of olivine (olv), pyroxene (px), feldspar (feld), and matrix (m). (A) The complete dissolution of an olivine grain was observed within 7 days. (B) The complete dissolution of an olivine grain occurred within 35 days.

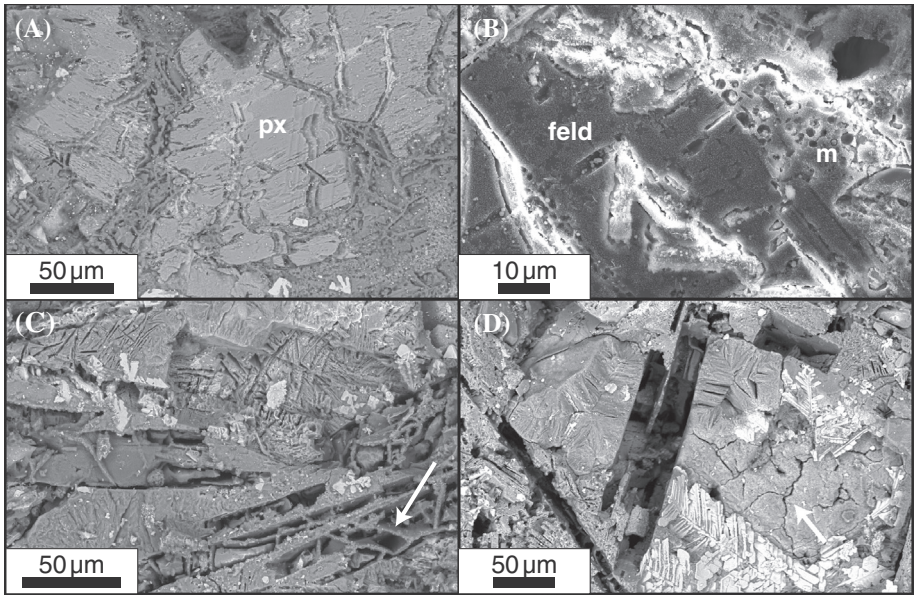

Fig. 4. Dissolution textures. (A) On the surface of Series 1 sample, after 7 days of reaction, evidence of dissolution occurred along pyroxene (px) grain boundaries and along microfractures. (B)–(D) The Series 2 sample, after 56 days of reaction, contained several distinct structures. (B) Circular features were common within the glassy matrix. (C) Fracture material (arrow) was preserved as feldspar grains dissolve, and irregular dissolution patterns (upper half of image) developed, which were similar to quench structures observed in unreacted glass matrix. (D) Complete dissolution of feldspar grains left tabular-shaped pits. Crack-like textures (arrow) also develop on the surface after the sample was dried. BSE images.

amount of 23.92 mg and 25.70 mg after 28 days and 56 days of reaction, respectively. In Series 2, the rate of release was higher within the initial stages of each series, with the rate slowing as the sample was progressively reacted. Since silicon is present in most minerals and matrix, except for ilmenite, the presence of silicon in the bulk solution best represents the dissolution of the basalt as a whole. The maximum Si release in a single increment (Series 2–35 weeks) was 8.69 g, and the maximum cumulative release was 25.70 g for Series 1. Amorphous silica, which has a solubility of 11 mM calculated from SUPCRT92, was present on the surface of the sample in small volumes. However, the limited amount of amorphous silica observed on the surface of the sample suggested that the amount precipitated from the bulk solution was small and was limited to a thin saturated layer just above the surface of the sample. The occurrences of other species in the final solutions represent the dissolution of specific minerals or groups of minerals and the glassy matrix. In decreasing order based on cumulative total release from silicon, Ca^{2+}, Mg^{2+}, Na^{+}, K^{+}, Fe^{2+}, and Mn^{2+} were also measured in the bulk solution (Fig. 2). Fluid chemistry was correlated to surface observations at each stage within Series 1 and Series 2 (Figs. 3, 4).

The release of Ca^{2+} must originate from pyroxene, plagioclase gains, or the glassy matrix. After 4 days of reaction from Series 1, Ca^{2+} released was less than the Mg^{2+} released, unlike the cumulative Ca^{2+} release observed in the first stage of Series 2, which was higher than the Mg^{2+} release. Dissolution was primarily observed at pyroxene grain boundaries and microfractures, with less extensive dissolution within plagioclase grains and matrix in Series 1 (Fig. 3A). Pyroxene and plagioclase dissolution was more noticeable (e.g., higher Ca^{2+} release, greater grain boundary dissolution) in the first stage of Series 2, which had 7 days to react, compared to Series 1. After 7 days of reaction in Series 1, large sections of pyroxene grains were dissolved, causing an increased Ca^{2+} release that was higher than the Mg^{2+} release. Entire portions of a pyroxene grain also dissolved in the Series 2 sample. These early stage observations suggest that Ca^{2+} primarily originates from the Ca-rich pyroxene grains, while contributions from plagioclase and matrix were minimal. After 7 days, dissolution is more obvious within the feldspar grains, resulting in a web-like pattern in both series (Fig. 4A). These textures correspond to a greater contribution of Ca^{2+} from plagioclase grains. After 56 days of reaction, several plagioclase grains (< 200 µm long) were also observed to have completely dissolved, leaving behind only the fracture-filled matrix (Fig. 4C, D), resulting in a greater contribution of Ca^{2+} to the solution. The final cumulative release of Ca^{2+} from the Series 1 and Series 2 tiles were 11.94 mg and18.43 mg, respectively.

The release of Mg^{2+} and Fe^{2+} could originate from either olivine or pyroxene grains. The formation of iron oxides on the surface of both samples, which was red after removal but before drying of the sample, most likely explains the relatively low cumulative release of Fe^{2+} observed throughout each series. Observations of the surface of each sample indicated that Fe-bearing minerals did react within the first 7 days; however, the precipitation of iron oxides reduced the total Fe^{2+} in the bulk solution. The iron oxides were distributed across the surface of the sample, and were < 0.5 µm in diameter. While Fe^{2+} remained generally low due to precipitation, the cumulative release of Mg^{2+} into solution resulted in up to 2.81 mg for Series 1 and 2.34 mg for Series 2 within the first 7 days of reaction. Based on the surface observations, small olivine grains (< 200 µm) were considerably dissolved away, while dissolution of pyroxene grains was limited to the grain boundaries and microfractures (Figs. 3A, 4A). The physical evidence of dissolution combined with the fluid chemistry indicates that most of the Mg^{2+} and Fe^{2+} observed within the first week originated from olivine grains, with only minor contributions from pyroxene grains. As Series 1 progressed the release of Mg^{2+} slowed, and the small olivine grains observed in both series completely dissolved within 2–3 weeks. The largest release in Series 2 occurred between 21 and 35 days of reaction when larger sections of pyroxene grains also dissolved, indicating that both olivine and pyroxene contributed to Mg^{2+} and Fe^{2+} into solution.

A possible indicator of plagioclase dissolution was the occurrence of Al^{3+} within the bulk solution. Aluminum was observed at low concentrations (< 0.1 mg) in all increments. The low accumulations would suggest that Al-bearing minerals were the least reactive. However, the precipitation of Al-bearing, platy crystals approximately 1 µm in size (Figs. 4D, 5) indicate that the Al^{3+} totals of the bulk solution do not adequately represent the dissolution of Al-bearing minerals. After the samples were dried for analysis, mounds (~5 µm from the surface of the sample) of the precipitates exhibited a texture similar to mud-cracks (Fig. 5D). Based on models of a steady-state reaction, the precipitation of diaspore (AlO(OH)) and/or gibbsite ($Al(OH)_3$) is possible at the low pH conditions obtained in these experiments (SI Fig. S3), and can be found in naturally weathered basalt (Dontsova et al., 2014; Liu et al., 2013; Stefansson and Gislason, 2001). Due to the small volume of the platy material, additional compositional analysis and identification was not possible.

The best evidence for feldspar dissolution and matrix dissolution

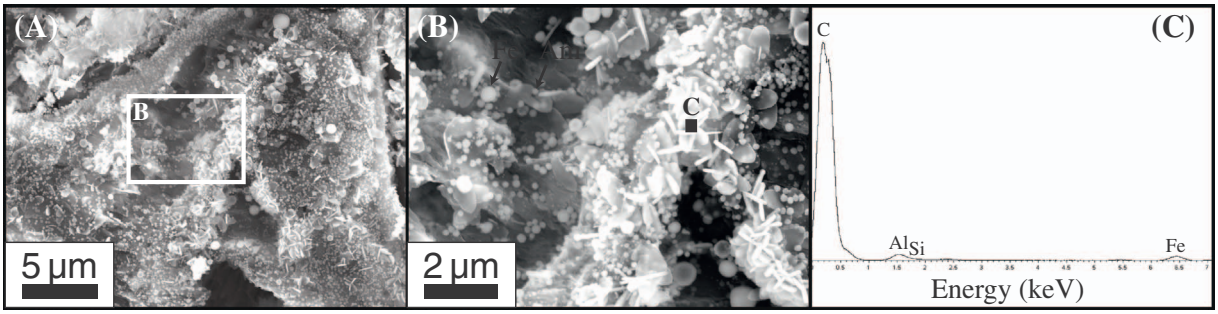

Fig. 5. Secondary precipitates. (A)–(B) BSE images of platy precipitates were observed on the surface of the Series 2 sample after 7 days of reaction. Iron oxides (Fe) and amorphous silica (Am) were also observed on the surface. (C) EDS spectra indicated precipitates were composed of aluminum.

was the release of Na^+ to the bulk solution. While Na^+ occurs with Ca^{2+} in plagioclase grains, the rate of release was not the same in the initial stages of Series 1. Sodium release was slower compared to Ca^{2+}, though faster than K^+. Most of the dissolution of plagioclase within the early stages occurred near the grain boundaries and along microfractures. The only evidence of dissolution observed within the matrix were pits (7 days of reaction, Series 1), but their occurrence was not associated with sodium release. Larger portions of plagioclase grains dissolved away after 16 and 21 days of reaction for Series 1 and Series 2, respectively. Entire plagioclase grains dissolved after 56 days of reaction, and distinct dissolution along twin boundaries were also observed on remaining feldspar grains (Fig. 4C, D). Additional evidence of dissolution occurs within the matrix along the Na-rich quench structures (SI Fig. S1; Fig. 4C). The final cumulative total of Na^+ in the bulk solution was 2.85 and 7.81 mg for Series 1 and Series 2, respectively.

The K^+ originated from the glassy matrix, as this was the only possible source. The total release of K^+ for each series remained low, resulting in total accumulations of 2.85 and 5.35 mg for the Series 1 sample and the Series 2 sample, respectively. Initial evidence of dissolution within the matrix was limited to the small pits. Even after 56 days of reaction for the Series 2 sample, the majority of the dissolution occurred within the pits or along the Na-rich quench structures.

4.2. Surface roughness

The surface of the Series 1 sample and the Series 2 sample increased in roughness after reaction in the CO_2-rich environment (Figs. 6, 7, 8). In each initial transect for each sample, some of the natural porosity was observed as small pits (< 20 μm deep), which increases the initial roughness quantities. Series 1 had initial Ra and RMS values of 0.2 and 0.4, respectively. The initial Series 2 tile was slightly rougher than the Series 1 tile, with Ra and RMS values of 0.39 and 0.75, respectively. A polished basalt sample analyzed with 3D methods had a surface roughness (Sa) of 0.21.

In both series, dissolution occurred in localized areas on the surface of each sample during the first 7 days of reaction, which resulted in the formation of pits. In comparison to the starting surface, the density and depth of pits increased within 1 day of reaction. While the average depth of pits only slightly increased to ~26 μm below the starting surface, the number of pits and width of the opening increased. The remainder of the surface of each sample stayed relatively smooth (Fig. 8). Based on SEM images, the newly formed pits formed as a result of partial dissolution of olivine grains (Fig. 3A). After 4 days of reaction, slight variations developed on the surface along grain boundaries and microfractures of the Series 1 sample, which increased the overall Ra and RMS values by a factor of 2.8 and 3.7, respectively (Figs. 3A, 6, 8). The continued development of large pits (Fig. 7B), now up to 109 μm below the starting surface, represented the continued dissolution of olivine grains. While localized pits resulted in a rather sharp increase in Ra and RMS values, the surface area only increased by 2.1%. The number of pits on the surface of each sample increased after 7 cumulative days of reaction for both series, and have an average depth of 60 μm (Series 1 sample) and 43 μm (Series 2 sample) (Fig. 6). This pit formation resulted in a surface area increase of 9.3% and 7.3% for the Series 1 sample and the Series 2 sample, respectively, from the initial polished surfaces (Fig. 8). For the remaining experiments of each series, Ra and RMS values were greater for the Series 1 sample than for the Series 2 sample.

After the first week of reaction, the rate of change in surface roughness slowed for both series. The pit density and general surface variability increased on the surface of each sample, after 16 and 21 days of reaction, which increased Ra and RMS values (Fig. 8). The complete dissolution of olivine grains and the continuing dissolution along grain boundaries, particularly around pyroxene grains, most likely contributed to the increases in roughness and surface area of 11.5% and 8.6% for the Series 1 sample and the Series 2 sample, respectively. In addition to the greater density and deepening of the pits, some pits also appeared to be wider (Fig. 8). These wider pits could be the result of larger grains dissolving away or of the continued dissolution of adjoining grains resulted in a merging of two pits. From 28 to 56 days of reaction, the general surface irregularities of each sample increased to 5–20 μm deep, and the Ra and RMS values increased as a result (Fig. 8). The final Ra and RMS value for the Series 1 sample after 28 cumulative days of reaction was 10.7 and 13.53, an increase by a factor of 53.5 and 33.8, respectively, and a total surface area increase of 14.9%. After a cumulative total of 56 days of reaction for the Series 2 sample, the Ra and RMS values increased to 10.7 and 13.53, an increase by a factor of 30.9 and 24.2, respectively, and a measured Sa value of 5.54 was also recorded (Fig. 7C). The final surface area increased by 20.0%. The main contribution to the final increase in roughness for both samples was from the complete dissolution of olivine grains, small plagioclase grains, and the general dissolution of the matrix, which finally started to show considerable evidence of dissolution. The formation of Al-oxides and Fe-oxides on the surface of the samples is mounds up to 5 μm thick could also influenced the roughness measurements (Fig. 6).

5. Discussion

5.1. Mineral dissolution and fluid chemistry

Ca^{2+}, Mg^{2+}, and Fe^{2+} cations, which are released during the dissolution of basalt, are significant due to their capacity to react with dissolved inorganic carbon to form carbonates. While these experiments do not represent steady-state reactions that are often used for dissolution rate experiments, they exhibit similar chemical trends to other steady-state experiments using basalt (Gudbrandsson et al., 2011; Schaef and McGrail, 2009; Wolff-Boenisch et al., 2011) that can be specifically linked to their source and surface dissolution patterns. Within the first 24 h, Mg^{2+} release dominates over Ca^{2+} release, which coincides with dissolution of either olivine and/or pyroxene grains, which is consistent with the dissolution rates of these minerals (Schott

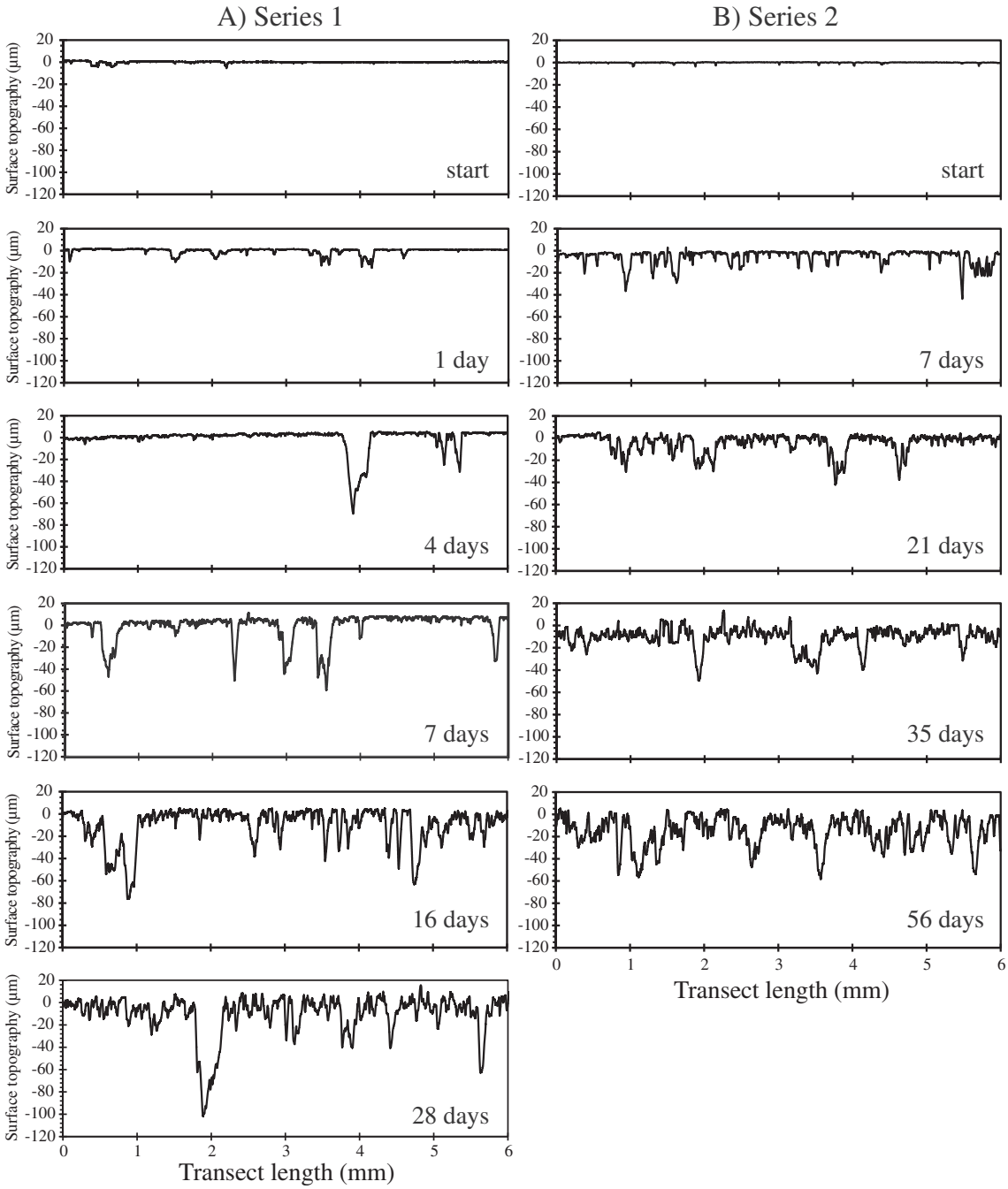

Fig. 6. Surface roughness evolution. 2D profilometer transects after each experiment for (A) Series 1 and (B) Series 2.

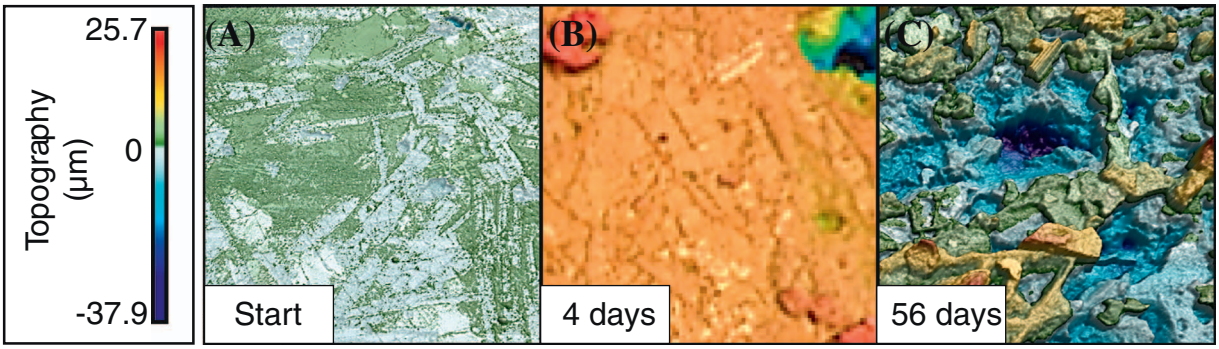

Fig. 7. Surface roughness. Topographic images of a 200 × 200 μm area from (A) a polished, unreacted surface, (B) Series 1 sample after 4 days of reaction, and (C) Series 2 sample after 56 days of reaction.

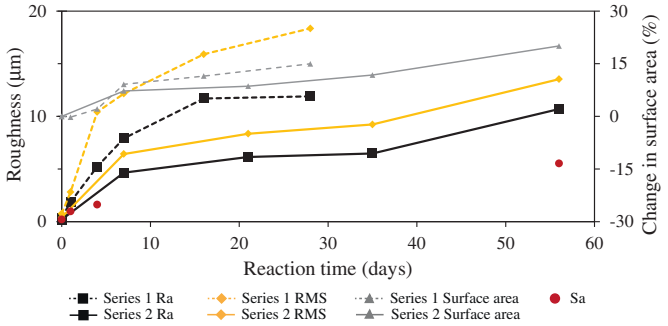

Fig. 8. Roughness measurements. Mean roughness (Ra), root mean squared (RMS), and mean surface area roughness (Sa) were calculated from each 2D profilometer transects and the laser confocal microscope. Surface area change was calculated using the actual transect length following each reaction period, and the starting horizontal length of the polished tile.

et al., 2009). Basalt dissolution in which no secondary precipitation was observed documented Fe^{2+} concentrations similar to Mg^{2+} concentrations (Gudbrandsson et al., 2011; Schaef and McGrail, 2009). However, in this study, remaining oxygen within the system resulted in the precipitation of iron oxides, which kept Fe^{2+} concentration near zero. Based on the limited Ca^{2+} within the solution and visual confirmation of dissolved olivine grains, the main contributor of Mg^{2+} and Fe^{2+} to the bulk solution within the initial stages of basalt dissolution is olivine. In steady-state reactions at low pH, Mg^{2+} and Fe^{2+} are expected to dominate (Gudbrandsson et al., 2011; Rogers et al., 2006). However, after the initial release of Mg^{2+} in this study, Mg^{2+} release slowed relative to Ca^{2+}, resulting in greater cumulative totals of Ca^{2+} after 7 days of reaction (Series 1 sample). The Ca^{2+}-Mg^{2+} switch observed in Series 1 may be the result of a slight increase in pH or a reduction in a mineral source (i.e., less olivine available for reaction). Dissolution rates tend to decrease as the bulk solution becomes more basic (pH 4–6) (Gudbrandsson et al., 2011); however, the overall pH remained acidic particularly during this transition (Fig. 1B). More than likely the cause of the lower Mg^{2+} release following 4–7 days of reaction was the depletion of minerals that were Mg^{2+} sources (i.e., olivine grains). In the initial stages of the reaction, this small component (9% modal volume) was the dominant contributor due to olivine's fast dissolution rate and small grain size. Once the reaction progressed past the initial olivine dissolution spike, pyroxene dissolution dominated the system, and Ca^{2+} became the dominant divalent metal cation observed in the bulk solution for the remainder of the series.

These observations suggest that while olivine is an ideal source for Mg^{2+} and Fe^{2+}, unless the basalt has large volumes of olivine, pyroxene will most likely be the continuing source of Mg^{2+}, Fe^{2+}, and even Ca^{2+}. Current carbon sequestration sites in large basalt formations (e.g., flood basalts) in Iceland (Franzson et al., 2008) and in the Columbia River Flood Basalt group (McGrail et al., 2011; Wells et al., 2016) have < 15% olivine in the total mineral volume. While no carbonates were observed in either series in this study, Ca- and Mg-bearing siderite precipitated within diffusion limited zones after 28 days of reaction in packed-powder bed experiments using the same material used in this study (Xiong et al., 2017). The continued dissolution of pyroxene in particular could then result in greater Ca^{2+} concentrations within the bulk solution, later resulting in the formation of more Ca-rich carbonates. Recent pilot-scale carbon sequestration tests utilizing basalt reservoirs document Ca-rich precipitates (calcite; Matter et al., 2016) and Ca-Fe rich precipitates (ankerite; McGrail et al., 2017), which might indicate that pyroxene is an important source in these reservoirs.

The slow dissolution of plagioclase results in the presence of Na^{+} and Al^{3+} in the bulk solution. While cumulative Al^{3+} totals should occur at similar levels as other cation during dissolution (Schaef and McGrail, 2009), the precipitation of Al-bearing oxides (e.g., diaspore, gibbsite) removed Al^{3+} from the bulk solution (SI Fig. S2). In these experiments, the Na^{+} was the best indicator of plagioclase dissolution because Na^{+} was unaffected by precipitation and did not overlap with other mineral sources. In general, the rate of release of Na^{+} slowed as the reaction progressed. The slower dissolution of feldspar compared to other minerals present (i.e., olivine and pyroxene) was expected based on single grain dissolution experiments (Table 1; Carrol and Knauss, 2001; Chen and Brantley, 1997; Oelkers and Schott, 1995; Palandri and Kharaka, 2004). The slowing dissolution of feldspar might be the result of the slight increase in pH in the later increments (Fig. 1B–C) or the slight accumulation of Al^{3+} within the solution (Gudbrandsson et al., 2014; Schott et al., 2009). In steady-state experiments, the rate of dissolution slows as pH increases towards a value of 6 or is inhibited by the presence of Al^{3+} within the solution (Gudbrandsson et al., 2014; Schott et al., 2009). The precipitation of aluminum oxides on the top surface of each sample, in combination with a static system, could have enabled Al^{3+} to impede feldspar dissolution, particularly towards the end of each series when time intervals were longer. The slowing Na^{+} trend observed in this study may also be the result of Al-oxide precipitation on the surface, which might have interfered with plagioclase dissolution, or the narrow window in which the samples were reacted.

The slow dissolution of the glassy matrix resulted in the relatively slow release of K^{+}. In addition to the slow and continuously low release of K^{+}, evidence of dissolution of the matrix was gradually documented, with no large volumes of matrix dissolving away. The K-rich nature of the glassy matrix in this study suggests that the matrix was Si-poor (Wolff-Boenisch et al., 2006), which decreased the dissolution rate compared to previously studied basaltic glass. Even within the K-rich matrix, the Na-rich structures within the glass dissolve more readily. In basalts where glassy matrix is present, dissolution will occur along chemical heterogeneities, resulting in irregular dissolution surfaces.

5.2. Effect of dissolution on surface morphology

For many experiments, the material used to quantify and observe dissolution processes consists of fine-grained powder with a quantified Brunauer-Emmett-Teller (BET) surface area. The surface area of these samples was sufficiently high to get representative surface area-normalized dissolution rates (Gudbrandsson et al., 2011; Schaef and McGrail, 2009). The samples reacted in this study remained intact with natural grain boundaries and considerably smaller surface areas compared to studies using powdered basalts (e.g., 7.75 $m^2\ g^{-1}$; Schaef and McGrail, 2009). In natural basalt reservoirs with smaller exposed surface areas, the total release of important divalent metal cations may be considerably lower than observed release totals in laboratory experiments. Reactive transport models that make all surfaces available for reaction must reduce the total reactive surface area by a factor of 10–20 for dissolved cations to be comparable to natural systems (Beckingham et al., 2017). Measured surface areas are typically applied to the starting conditions; however, the surface area of the reservoir will change as dissolution proceeds. There may also be pre-existing structures (e.g., quench structures, grain boundaries, fractures) within the basalt that may also preferentially react in ways that alter the total surface area exposed to the CO_2-rich environment.

The reaction of intact basalt samples in a CO_2-rich environment could increase the surface area of the basalt by a factor of 1.2 in acidic conditions. This increase will expose more material and increase the total release of material. Increasing surface area, particularly pyroxene with exposed Ca-Mg-Fe bonds, could also act as a starting substrate for carbonate growth if these mineral surfaces are still available once carbonate precipitation begins (i.e., the minerals are not completely dissolved away) (Stockmann et al., 2014). In this study, the overall surface area of the Series 1 sample and the Series 2 sample increased by approximately the same amount despite different interval and overall reaction times, and each roughness parameter increased by a factor > 10. In studies that examined dissolution of artificially and naturally weathered powdered materials (e.g., feldspars, clays), the

surface area increased by a factor of 1–2 orders of magnitude compared to the artificially smooth starting material (Anbeek, 1992; Black et al., 2015; Metz et al., 2005; Stillings and Brantley, 1995). The difference in surface area between the starting material and reacted material may influence the total release of cations to the bulk solution. In the case where the difference in surface area was a factor of 2.6, the release of total silicon was slightly lower when the surface area was smaller (Schaef and McGrail, 2009; Wolff-Boenisch et al., 2006). While the roughness and surface area increased over time, the total release of silicon and important divalent metal cations slowed despite remaining in acidic conditions. The decreasing release may be the result of slight increase in pH that resulted in slowing dissolution rates for some minerals. However, despite the different pH paths (calculated from measured cation concentrations) (Fig. 1B–C), both series experienced similar decreasing release. In flow-through experiments using the same flood basalt used in this study, cation release decreases towards a steady-state within the first 24 h from the start of the reaction (Adeoye et al., 2017). This decrease is similar to what is observed in our study. The slowing release could also indicate that the rate of exposure of new minerals could not compete with the rate of loss of important mineral sources (e.g., olivine and pyroxene grains). The initial dissolution of olivine grains and considerable portions of pyroxene grains contributed to the surface area increase, but the remaining minerals and matrix dissolved slowly, resulting in lower totals in the bulk solution. For concentrations to increase, dissolution processes will have to compete with an increasing pH, which slows dissolution near neutral conditions (Gudbrandsson et al., 2011; Schaef and McGrail, 2009; Wolff-Boenisch et al., 2006), and expose additional olivine and pyroxene grains to keep Ca^{2+}, Mg^{2+}, and Fe^{2+} concentrations elevated.

In initial stages of dissolution, increased roughness and surface area occurs primarily along original grain boundaries and along pre-existing microfractures. While the development of dissolution textures in specific minerals (Anbeek, 1992; Gislason and Oelkers, 2003; Gudbrandsson et al., 2014; Saldi et al., 2015) and along pre-existing structures (Haug et al., 2010) is common, an examination of intact samples indicates a considerable amount of dissolution will initiate at grain boundaries and along microfractures, which can be common within basalt formation. Such small structures contribute to the variable surface roughness, ranging up to 10 μm, but do little to influence large pit formations, and at least initially have a minimal impact on total dissolved species as the newly exposed surface area is too small. However, the evolution of these rather small features (< 2 m) to larger openings (5–10 μm) could eventually open new passageways to reactive minerals or could offer more surface area on which precipitates could nucleate (Garcia et al., 2010; Stockmann et al., 2014). These narrows zones could eventually act as diffusion limited zones when the solution is saturated enough to initiate precipitation of carbonates (Giammar et al., 2014; Xiong and Giammar, 2014). Eventually, small circular marks and dissolved quench structures (Na-rich areas) also form in the matrix, and web-like patterns appear within feldspar grains. The total contribution of dissolution along grain boundaries, microfractures, or within the matrix to the overall roughness (Ra and RMS parameters) is quite small compared to the formation of larger pits left behind from dissolution of entire grains.

The greatest influence on the roughness of a basalt wall and the total dissolved species within a reservoir would be from the significant dissolution of grains. Small olivine grains completely dissolve within the first 1–2 weeks, while pyroxene grains never fully dissolve in the observed areas, though there are smaller grains that could be completely dissolved within the observed reaction time. As a result of the complete dissolution of olivine and possibly pyroxene grains, the sharpest increase in roughness occurred (Fig. 8) resulting an increase in porosity that could expose more reactive surfaces. If new olivine grains or pyroxene grains are exposed, then these grains could further dissolve and provide divalent metal cations (e.g., Ca^{2+}, Mg^{2+}, and Fe^{2+}). In turn, as more material is exposed for dissolution, more cations will be released into the solution that could be used for carbonate precipitation. For olivine and pyroxene to dissolve and reveal significantly more material, the modal volume for each mineral would need to be at least 28%, based on percolation thresholds for ellipsoids (Garboczi et al., 1995) for each. However, olivine and pyroxene only make up 9% and 22%, respectively, of the basalt studied here. The low modal volume and rounded grains indicates that while these grains will readily dissolve over time, the limited connectivity may limit the extent of dissolution into the basalt. However, other basalt reservoirs with greater modal abundances of olivine or pyroxene may reach this percolation threshold. Plagioclase grains are more elongated and make up 31% of the modal volume. The more ellipsoid shape of these grains lowers the percolation threshold to 26% (Garboczi et al., 1995); however, the dissolution rate for plagioclase is relatively slow. In a natural system, the fluids will eventually become saturated and precipitation will occur on the surface of the basalt. The available reactive surface area will decrease once carbonates begin to precipitate. The precipitation of aluminum and iron oxides within each series indicates that some surfaces will become covered and impede dissolution. However, the observed oxides are small and do not cover large portions of the surface. In experimental studies at similar conditions, carbonate precipitation can occur within 4–6 weeks within diffusion limited zones (Xiong et al., 2017), while precipitate can occur within 2 years in natural basalt reservoirs at lower temperatures (Matter et al., 2016; McGrail et al., 2017).

6. Conclusion

Olivine is often considered as the main source for divalent metal cations in basalt formations, particularly when carbonation is the primary goal for permanent carbon storage. However, by examining dissolved cations in solution and the reacted surface area over incremented time periods, this study indicates that the slightly slower dissolution of pyroxene compared to olivine and higher modal volume act as a sustained source for several divalent metal cations (Ca^{2+}, Fe^{2+}, and Mg^{2+}) that can be used in carbonation reactions. The early stages of dissolution of a Columbia River flood basalt sample indicated a relatively fast (i.e., within 4 days at higher temperatures and acidic conditions) transition from olivine being the dominant Mg^{2+} and Fe^{2+} contributor to pyroxene being the dominant contributor. Pyroxene was more common, and continued to react through a cumulative 28 and 56 days of reaction in each series. As olivine grains are dissolved, more dissolution is observed along grain boundaries and microfractures within pyroxene and plagioclase grains. Some dissolution was observed within the glass K-rich matrix; however, the contribution from the glass matrix remained minimal. The results of this study indicate basalts with larger modal volumes of pyroxene should be considered as the target mineral for carbon sequestration in basalt reservoirs.

The surface evolution observed in each series indicates preferential dissolution will increase the surface area by a factor of ~1.2. However, due to the limited connectivity of the olivine and pyroxene grains, significant exposure of additional grains does not occur. Based on our observations, basalt dissolution associated with carbon storage will be heterogeneous, resulting in localized pits instead of general dissolution of the basalt. In early stages, dissolution of small olivine grains (< 200 μm) resulted in large pits. As dissolution continues, smaller textures associated with dissolution along grain boundaries, microfractures, and pre-existing structures (e.g., quench structures within the matrix) and larger pits formed. As a result of the dissolution, the surface roughness parameters, Ra and RMS values, increased by a factor of 43.7 and 28.9, respectively. A quantification of the surface roughness indicates, to some degree, how the surface area will evolve, which could influence dissolution rates in addition to the external conditions (e.g., temperature, pH) of the reservoir. While the surface roughness increased overall and large pits significant enough to exposes more minerals occurred, the low connectivity of Ca-, Fe-, and Mg-bearing

sources was not sufficient to continue supplying important divalent metal cations. As a result, the rate of release of important divalent metal cations slowed as the reaction progressed.

Acknowledgements

This material is based upon work supported by the Department of Energy under Award Number DE-FE0023382. Electron microscopy was supported by the Institute of Materials Science and Engineering at Washington University in St. Louis. We would like to thank two anonymous reviewers for their reviews of the manuscript.

Appendix A. Supplementary data

Supplementary data to this article can be found online at http://dx.doi.org/10.1016/j.chemgeo.2017.07.028.

References

Adeoye, J.T., Menefee, A.H., Xiong, W., Wells, R.K., Skemer, P., Giammar, D.E., Ellis, B.R., 2017. Effect of transport limitations and fluid properties on reaction products in fractures of unaltered and serpentinized basalt exposed to high P_{CO2} fluids. Int. J. Greenhouse Gas Control 63, 310–320.

Anbeek, C., 1992. Surface roughness of minerals and implications for dissolution studies. Geochim. Cosmochim. Acta 56, 1461–1469.

Andreani, M., Luquot, L., Gouze, P., Godard, M., Gibert, B., 2009. Experimental study of carbon sequestration reactions controlled by the percolation of CO_2-rich brine through peridotites. Environ. Sci. Technol. 43, 1226–1231.

Beckingham, L.E., Steefel, C.I., Swift, A.M., Voltolini, M., Yang, L., Anovitz, L., Sheets, J.M., Cole, D.R., Kneafsey, T.J., Mitnick, E.H., Zhang, S., Landrot, G., Ajo-Franklin, J., DePaolo, D., Mito, S., Xue, Z., 2017. Evaluation of accessible mineral surface areas for improved prediction of mineral reaction rates in porous media. Geochim. Cosmochim. Acta 205, 31–49.

Black, J.R., Carroll, S.A., Haese, R.R., 2015. Rates of mineral dissolution under CO_2 storage conditions. Chem. Geol. 399, 134–144.

Carrol, S.A., Knauss, K.G., 2001. Experimental determination of Ca-silicate dissolution rates: a source of calcium for geologic CO_2 sequestration. In: DOE/NETL First National Conference on Carbon Sequestration. Washington, DC, pp. 1–17.

Chen, Y., Brantley, S.L., 1997. Temperature- and pH-dependence of albite dissolution rate at acid pH. Chem. Geol. 135, 275–290.

Dixit, S., Carroll, S.A., 2007. Effect of solution saturation state and temperature on diopside dissolution. Geochem. Trans. 8, 1–14.

Dontsova, K., Zaharescu, D., Henderson, W., Verghese, S., Perdrial, N., Hunt, E., Chorover, J., 2014. Impact of organic carbon on weathering and chemical denudation of granular basalt. Geochim. Cosmochim. Acta 139, 508–526.

Duan, Z., Sun, R., 2003. An improved model calculating CO_2 solubility in pure water and aqueous NaCl solutions from 273 to 533 K and from 0 to 2000 bar. Chem. Geol. 193, 257–271.

Elkhoury, J.E., Ameli, P., Detwiler, R.L., 2013. Dissolution and deformation in fractured carbonates caused by flow of CO_2-rich brine under reservoir conditions. Int. J. Greenhouse Gas Control 16, S203–S215.

Ellis, B.R., Fitts, J.P., Bromhal, G.S., Mcintyre, D.L., Tappero, R., Peters, C.A., 2013. Dissolution-driven permeability reduction of a fractured carbonate caprock. Environ. Eng. Sci. 30, 187–193.

Franzson, H., Zierenberg, R., Schiffman, P., 2008. Chemical transport in geothermal systems in Iceland. Evidence from hydrothermal alteration. J. Volcanol. Geotherm. Res. 173, 217–229.

Garboczi, E.J., Snyder, K.A., Douglas, J.F., 1995. Geometrical percolation threshold of overlapping ellipsoids. Phys. Rev. E Stat. Phys. Plasmas Fluids Relat. Interdiscip. Topics 52, 819–828.

Garcia, B., Beaumont, V., Perfetti, E., Rouchon, V., Blanchet, D., Oger, P., Dromart, G., Huc, A.Y., Haeseler, F., 2010. Experiments and geochemical modelling of CO_2 sequestration by olivine: potential, quantification. Appl. Geochem. 25, 1383–1396.

Giammar, D.E., Wang, F., Guo, B., Surface, J.A., Peters, C.A., Conradi, M.S., Hayes, S.E., 2014. Impacts of diffusive transport on carbonate mineral formation from magnesium silicate-CO_2-water reactions. Environ. Sci. Technol. 48, 14344–14351.

Gislason, S.R., Oelkers, E.H., 2003. Mechanism, rates, and consequences of basaltic glass dissolution: II. An experimental study of the dissolution rates of basaltic glass as a function of pH and temperature. Geochim. Cosmochim. Acta 67, 3817–3832.

Gudbrandsson, S., Gíslason, S.R., Wolff-Boenisch, D., Oelkers, E.H., 2008. Dissolution rates of crystalline basalt at pH 4 and 10 and 25–75 °C. Mineral. Mag. 72, 155–158.

Gudbrandsson, S., Wolff-Boenisch, D., Gislason, S.R., Oelkers, E.H., 2011. An experimental study of crystalline basalt dissolution from $2 < pH < 1$ and temperatures from 5 to 75 °C. Geochim. Cosmochim. Acta 75, 5496–5509.

Gudbrandsson, S., Wolff-boenisch, D., Gislason, S.R., 2014. Experimental determination of plagioclase dissolution rates as a function of its composition and pH at 22 °C. Geochim. Cosmochim. Acta 139, 154–172.

Haug, T.A., Kleiv, R.A., Munz, I.A., 2010. Investigating dissolution of mechanically activated olivine for carbonation purposes. Appl. Geochem. 25, 1547–1563.

IPCC, 2005. IPCC Special Report on Carbon Dioxide Capture and Storage. Prepared by Working Group III of the Intergovernmental Panel on Climage Change. Cambridge University Press, Cambridge, United Kingdom and New York, NY, USA.

Kelemen, P.B., Matter, J., 2008. In situ carbonation of peridotite for CO_2 storage. Proc. Natl. Acad. Sci. U. S. A. 105, 17295–17300.

Liu, X., Rudnick, R.L., Mcdonough, W.F., Cummings, M.L., 2013. Influence of chemical weathering on the composition of the continental crust: insights from Li and Nd isotopes in bauxite profiles developed on Columbia River Basalts. Geochim. Cosmochim. Acta 115, 73–91.

Luhmann, A.J., Tutolo, B.M., Tan, C., Moskowitz, B.M., Saar, M.O., Seyfried, W.E., 2017. Whole rock basalt alteration from CO_2-rich brine during flow-through experiments at 150 °C and 150 bar. Chem. Geol. 453, 92–110.

Matter, J.M., Stute, M., Snæbjornsdottir, S.O., Oelkers, E.H., Gislason, S.R., Aradottir, E.S., Sigfusson, B., Gunnarsson, I., Alfredsson, H.A., Wolff-boenisch, D., Mesfin, K., Dideriksen, K., Broecker, W.S., 2016. Rapid carbon mineralization for permanent disposal of anthropogenic carbon dioxide emissions. Science 352, 10–13 (80-.).

McGrail, B.P., Spane, F.A., Sullivan, E.C., Bacon, D.H., Hund, G., 2011. The Wallula basalt sequestration pilot project. Energy Procedia 4, 5653–5660.

McGrail, B.P., Schaef, H.T., Spane, F.A., Cli, J.B., Qafoku, O., Horner, J.A., Thompson, C.J., Owen, A.T., Sullivan, C.E., 2017. Field validation of supercritical CO_2 reactivity with basalts. Environ. Sci. Technol. Lett. 4, 6–10.

Metz, V., Raanan, H., Pieper, H., Bosbach, D., Ganor, J., 2005. Towards the establishment of a reliable proxy for the reactive surface area of smectite. Geochim. Cosmochim. Acta 69, 2581–2591.

Oelkers, E.H., Schott, J., 1995. Experimental study of anorthite dissolution and the relative mechanism of feldspar hydrolysis. Geochim. Cosmochim. Acta 59, 5039–5053.

Olsson, J., Bovet, N., Makovicky, E., Bechgaard, K., Balogh, Z., Stipp, S.L.S., 2012. Olivine reactivity with CO_2 and H_2O on a microscale: implications for carbon sequestration. Geochim. Cosmochim. Acta 77, 86–97.

Palandri, J.L., Kharaka, Y.K., 2004. A Compilation of Rate Parameters of Water-mineral Interaction Kinetics for Application to Geochemical Modeling. National Energy Technology Laboratory, United States Department of Energy U.S. Dept. of the Interior, U.S. Geological Survey Menlo Park, Calif.

Petropoulos, G.P., Pandazaras, C.N., Davim, J.P., 2010. Surface texture characterization and evaluation related to machining. In: Davim, J.P. (Ed.), Surface Integrity in Machining. Springer-Verlag London, pp. 215.

Peuble, S., Godard, M., Luquot, L., Andreani, M., Martinez, I., Gouze, P., 2015. CO_2 geological storage in olivine rich basaltic aquifers: new insights from reactive-percolation experiments. Appl. Geochem. 52, 174–190.

Qafoku, O., Kovarik, L., Kukkadapu, R.K., Ilton, E.S., Arey, B.W., Tucek, J., Felmy, A.R., 2012. Fayalite dissolution and siderite formation in water-saturated supercritical CO_2. Chem. Geol. 332–333, 124–135.

Rimstidt, J.D., Brantley, S.L., Olsen, A.A., 2012. Systematic review of forsterite dissolution rate data. Geochim. Cosmochim. Acta 99, 159–178.

Rogers, K.L., Neuhoff, P.S., Pedersen, A.K., Bird, D.K., 2006. CO_2 metasomatism in a basalt-hosted petroleum reservoir. Lithos 92, 55–82.

Saldi, G.D., Daval, D., Guo, H., Guyot, F., Bernard, S., Le Guillou, C., Davis, J.A., Knauss, K.G., 2015. Mineralogical evolution of Fe – Si-rich layers at the olivine-water interface during carbonation reactions. Am. Mineral. 100, 2655–2669.

Schaef, T.H., McGrail, P.B., 2009. Dissolution of Columbia River Basalt under mildly acidic conditions as a function of temperature: experimental results relevant to the geological sequestration of carbon dioxide. Appl. Geochem. 24, 980–987.

Schott, J., Pokrovsky, O.S., Oelkers, E.H., 2009. The link between mineral dissolution/precipitation kinetics and solution chemistry. Rev. Mineral. Chem. 70, 207–258. http://dx.doi.org/10.2138/rmg.2009.70.6.

Singurindy, O., Berkowitz, B., 2005. The role of fractures on coupled dissolution and precipitation patterns in carbonate rocks. Adv. Water Resour. 28, 507–521.

Stefansson, A., Gislason, S.R., 2001. Chemical weathering of basalts, southwest Iceland: effect of rock crystallinity and secondary minerals on chemical fluxes to the ocean. Am. J. Sci. 301, 513–556.

Stillings, L.L., Brantley, S.L., 1995. Feldspar dissolution at 25 °C and pH 3: reaction stoichiometry and the effect of cations. Geochim. Cosmochim. Acta 59, 1483–1496.

Stockmann, G.J., Wolff-boenisch, D., Bovet, N., Gislason, S.R., Oelkers, E.H., 2014. The role of silicate surfaces on calcite precipitation kinetics. Geochim. Cosmochim. Acta 135, 231–250.

Wells, R.K., Giammar, D., Skemer, P., 2016. Sample Library of Natural and Artifical Basalts.

Wells, R.K., Xiong, W., Sesti, E., Cui, J., Giammar, D., Skemer, P., Hayes, S.E., Conradi, M.S., 2017. Spatially-variable Carbonation Reactions in Polycrystalline Olivine. 204. pp. 252–266.

White, A.F., Peterson, M.L., Hochella Jr, M.F., 1994. Electrochemistry and dissolution kinetics of magnetite and ilmenite. Ceochim. Cosmochim. Acta 58, 1859–1875.

Wolff-Boenisch, D., Gislason, S.R., Oelkers, E.H., 2006. The effect of crystallinity on dissolution rates and CO_2 consumption capacity of silicates. Geochim. Cosmochim. Acta 70, 858–870.

Wolff-Boenisch, D., Wenau, S., Gislason, S.R., Oelkers, E.H., 2011. Dissolution of basalts and peridotite in seawater, in the presence of ligands, and CO_2: implications for mineral sequestration of carbon dioxide. Geochim. Cosmochim. Acta 75, 5510–5525.

Xiong, W., Giammar, D., 2014. Forsterite carbonation in zones with transport limited by diffusion. Environ. Sci. Technol. Lett. 1, 333–338.

Xiong, W., Wells, R.K., Giammar, D.E., 2017. Carbon sequestration in olivine and basalt powder packed beds. Environ. Sci. Technol. 51, 2105–2112.